Available online at www.sciencedirect.com
ScienceDirect
International Journal of Mass Spectrometry 267 (2007) 233–247
International Journal of Mass Spectrometry
www.elsevier.com/locate/ijms

Cation-π interactions with a π-excessive nitrogen heterocycle: Structures and absolute binding energies of alkali metal cation–pyrrole complexes

Chunhai Ruan, Zhibo Yang, M.T. Rodgers *

Department of Chemistry, Wayne State University, Detroit, MI 48202, United States

Received 3 October 2006; received in revised form 9 February 2007; accepted 21 February 2007
Available online 25 February 2007

Dedicated to the memory of Sharon G. Lias, in thanks for her many contributions to gas phase ion thermochemistry and the NIST thermochemistry databases.

Abstract

Threshold collision-induced dissociation techniques are employed to determine the bond dissociation energies (BDEs) of mono- and bis-complexes of alkali metal cations, Na^+, K^+, Rb^+, Cs^+, and the bis-complex of Li^+, with pyrrole, C_4H_5N. The primary and lowest energy dissociation pathway in all cases is the endothermic loss of an intact pyrrole ligand. Sequential loss of a second pyrrole ligand is observed at elevated energies for the bis-complexes. Theoretical calculations at the MP2(full)/6-31G* level of theory are used to determine the structures, vibrational frequencies, and rotational constants of these complexes. Theoretical BDEs are determined from single point energy calculations at the MP2(full)/6-311+G(2d,2p) level using the MP2(full)/6-31G* optimized geometries. The agreement between theory and experiment is good for all complexes. The nature of the binding and the trends in the BDEs of these alkali metal cation–pyrrole complexes are compared to the analogous benzene and indole complexes using electrostatic potential maps and natural bond orbital analyses to examine the influence of the size of the aromatic system and the nitrogen heteroatom on the cation-π interaction. The binding of alkali metal cations to pyrrole is also compared to other metal cations and organic cations.

Keywords: Alkali metal cations; Cation-π interactions; Collision-induced dissociation; Heterocycles; Pyrrole

1. Introduction

Noncovalent interactions are key determinants in the delicate balance of forces that control the three-dimensional structures of biological macromolecules, e.g., proteins, carbohydrates, and nucleic acids. Such noncovalent interactions also mediate processes such as receptor–ligand, enzyme–substrate, and antibody–antigen recognition. Compared to more conventional noncovalent interactions, e.g., hydrophobic interactions, hydrogen bonds, and salt bridges, cation-π interactions [1–5] along with charge-dipole [6,7] and π stacking [8,9] interactions were under appreciated until the pioneering work of Dougherty and co-workers [1–5]. Their studies led to widespread investigations of cation-π interactions involved in protein folding and assembly [1–5,10–14], the functioning of ion channels in membranes [15,16], and in various molecular recognition processes [17].

A large number of fundamental studies have been carried out to characterize the factors that control the binding geometry, strength, and specificity of cation-π interactions [18–34]. Cation-π interactions involving metal cations, particularly alkali metal cations, have been investigated most thoroughly because of their biological importance [22,24–31,33,34]. In spite of the biological importance of organic cations in many molecular recognition processes, few studies of cation-π interactions involving organic cations have been conducted [35,36]. Heteroatoms, such as O, N, and S, have greater electronegativities and more electron density than carbon, and can therefore significantly influence cation-π binding by delocalizing electron density into or withdrawing electron density from the π ring and thus play roles in vital biological processes that occur in living organisms, including enzymatic catalysis and signal conduction. Pyrrole is a nitrogen heterocycle that possesses an electron lone pair that is perpendicular to the aromatic ring that delocalizes its electron density into the π system, creating a π-excessive aromatic ring as compared to benzene (i.e., six π electron delocalized over five atoms rather than six atoms as in benzene). Both theory and experiments have been applied to study cation-

* Corresponding author. Tel.: +1 313 577 2431; fax: +1 313 577 8822.
E-mail address: mrodgers@chem.wayne.edu (M.T. Rodgers).

1387-3806/$ – see front matter © 2007 Elsevier B.V. All rights reserved.
doi:10.1016/j.ijms.2007.02.041

π interactions between pyrrole and various metal cations. In our previous work [31], we measured the bond dissociation energies (BDEs) of M^+ (pyrrole) complexes, where $M^+ = Li^+$, Na^+, and K^+, and found that the π bonding geometry is favored over σ bonding. Gapeev et al. measured the first and second binding energies of pyrrole to Mg^+, Al^+, and several transition metal cations, including Ti^+, V^+, Cr^+, Mn^+, Fe^+, Co^+, Ni^+, Cu^+, Mo^+, and W^+ using radiative association and ligand exchange methods [32]. The cation-π solvation of alkali and alkaline earth metal cations by pyrrole was also reported [37]. Similarly, binding of alkali metal cations to indole, the fused ring nitrogen heterocycle comprised of benzene and pyrrole rings, occurs preferentially to the π systems above the benzene ring (π6) and pyrrolyl ring (π5) over σ bonding. Studies of a lariat ether of indole as a model for Trp found that metal cations can be stabilized by interaction with the pyrrolyl ring over the phenyl ring as a result of steric limitations [38,39], a situation that may also occur during biological processes.

Aniline, *N*-methylaniline, and *N*,*N*-dimethylaniline are aromatic amines with a N heteroatom in the side chain. The electron lone pair of electrons on the N atom is aligned with the π electrons of the benzene ring and thus partially delocalizes electron density into the π system and thereby enhances cation-π interactions. Alkali metal cations also prefer π binding to these aromatic amines. The strength of binding in these alkali metal cation-π complexes is stronger than to benzene and pyrrole, and comparable to indole, as a result of delocalization of the N electron density into the π system, larger polarizability, and the component of the dipole moment perpendicular to the π system [28,33]. For other N heterocyclic aromatics, e.g., pyrazole [31], imidazole [31,40], 1,2,3-triazole [40], 1,2,4-triazole [40], tetrazole [40], and pyridine [41], at least one lone pair of electron(s) on the N heteroatom(s) lies in the plane of the aromatic ring. Because nitrogen is more electronegative than carbon and disturbs the symmetry of the molecule, more electron density is localized around the nitrogen thereby decreasing the resonant stabilization and aromatic character, making these molecules better proton or cation acceptors and less likely to form cation-π complexes. As a result, alkali metal cations prefer σ binding to the N heteroatom(s) in these π-deficient aromatic ligands.

Of the *N*-heterocycles, pyrrole appears in various biomolecules, e.g., porphyrins, bile pigments, and phycobilins [42]. As a π-excessive building block, pyrrole-containing compounds, e.g., indole and tryptophan (Trp), are significantly influenced by the presence of the N heteroatom. Among the aromatic amino acids, Trp is known to participate in cation-π interactions more frequently than phenylalanine (Phe) and tyrosine (Tyr) [5]. In previous work, we concluded that this preference is the result of both stronger binding of alkali metal cations to indole than to benzene and phenol as a result of the π-excessive nature of this ligand and the extended size of the π network. In order to further elucidate the influence of N on cation-π interactions of heterocyclic species, the preference for cation-π interactions involving Trp in proteins, and to characterize the nature and trends in the binding of alkali metal cations to pyrrole, detailed characterization of alkali metal cation–pyrrole interactions are performed here.

In the present study, the kinetic energy dependences of the collision-induced dissociation (CID) of $M^+(C_4H_5N)_x$ complexes, where $M^+ = Na^+$, K^+, Rb^+, and Cs^+ for $x = 1$ and 2, and Li^+ for $x = 2$, with Xe are examined using a guided ion beam tandem mass spectrometer. The kinetic energy dependent cross-sections for the primary CID processes observed for each complex are analyzed using methods previously developed [43]. The trends in the binding energies and the influence of the N heteroatom on cation-π binding are examined. The binding of alkali metal cations to pyrrole is compared with main group and transition metal cations, and to organic cations to examine the influence of the size and nature of the cation on the cation-π interaction.

2. Experimental and theoretical

2.1. Experimental protocol

Cross-sections for CID of $M^+(C_4H_5N)_x$, where $M^+ = Na^+$, K^+, Rb^+, and Cs^+ for $x = 1$ and 2, and Li^+ for $x = 2$, are measured using a guided ion beam tandem mass spectrometer that has been described in detail previously [44]. The complexes are generated in a flow tube ion source by condensation of the alkali metal cation and neutral pyrrole molecule(s). These complexes are collisionally stabilized and thermalized by in excess of 10^5 collisions with the He and Ar bath gases such that the internal energies of the ions emanating from the source region are well described by a Maxwell–Boltzmann distribution at room temperature. The ions are effusively sampled from the source, focused, accelerated, and focused into a magnetic sector momentum analyzer for mass analysis. Mass-selected ions are decelerated to a desired kinetic energy and focused into an octopole ion guide. The octopole passes through a static gas cell containing Xe at low pressure (0.05–0.20 mTorr) to ensure that multiple ion-neutral collisions are improbable. The octopole ion guide acts as an efficient trap for ions in the radial direction. Therefore, loss of scattered reactant and product ions in the octopole region is almost entirely eliminated [45–47]. Xe is used here, and in general for all of our CID measurements, because it is heavy and polarizable and therefore leads to more efficient kinetic to internal energy transfer in the CID process [48–50]. Product and unreacted beam ions drift to the end of the octopole where they are focused into a quadrupole mass filter for mass analysis and subsequently detected with a secondary electron scintillation detector and standard pulse counting techniques.

2.1.1. Data handling

Measured ion intensities are converted to absolute cross-sections using a Beers' law analysis as described previously [51]. Absolute uncertainties in cross-section magnitudes are estimated to be ±20%, which are largely the result of errors in the pressure measurement and the length of the interaction region. Relative uncertainties are approximately ±5%.

Ion kinetic energies in the laboratory frame, E_{lab}, are converted to energies in the center of mass frame, E_{CM}, using the formula $E_{CM} = E_{lab}m/(m + M)$, where M and m are the masses of the ionic and neutral reactants, respectively. All energies

Table 1
Vibrational frequencies and average internal energies of pyrrole and $M^+(C_4H_5N)_x$, $x = 1,2$[a]

Species	E_{int} (eV)[b]	Vibrational frequencies (cm^{-1})[c]
C_4H_5N	0.08 (0.02)	453, 571, 617, 618, 686, 750, 767, 850, 872, 1033, 1057, 1096, 1153, 1158, 1291, 1421, 1468, 1487, 1544, 3177, 3187, 3200, 3206, 3555
$Na^+(C_4H_5N)$	0.12 (0.02)	112, 146, 233, 572, 593, 663, 700, 756, 813, 833, 856, 873, 1027, 1051, 1091, 1135, 1157, 1286, 1401, 1440, 1468, 1520, 3178, 3186, 3198, 3202, 3504
$K^+(C_4H_5N)$	0.13 (0.02)	108, 136, 170, 555, 578, 652, 678, 738, 794, 808, 854, 873, 1030, 1054, 1093, 1141, 1158, 1288, 1410, 1447, 1473, 1528, 3175, 3184, 3197, 3201, 3510
$Rb^+(C_4H_5N)$	0.13 (0.02)	82, 113, 130, 545, 569, 644, 665, 728, 785, 795, 852, 872, 1030, 1054, 1093, 1144, 1158, 1289, 1413, 1454, 1477, 1531, 3174, 3183, 3197, 3201, 3515
$Cs^+(C_4H_5N)$	0.13 (0.01)	74, 107, 115, 539, 568, 640, 659, 723, 781, 792, 852, 872, 1031, 1055, 1093, 1145, 1158, 1290, 1415, 1456, 1479, 1534, 3173, 3183, 3197, 3201, 3519
$Li^+(C_4H_5N)_2$	0.25 (0.02)	64, 75, 109, 143, 144, 204, 275, 532, 572, 573, 579, 587, 667, 678, 702, 716, 761, 765, 817, 819, 826, 833, 857, 858, 872, 873, 1026, 1029, 1050, 1052, 1090, 1092, 1135, 1137, 1156, 1158, 1285(2), 1402, 1403, 1437, 1439, 1464, 1467, 1519, 1520, 3183(2), 3192(2), 3204(2), 3208(2), 3503(2)
$Na^+(C_4H_5N)_2$	0.27 (0.02)	18, 22, 85, 123, 131, 132, 163, 299, 561, 564, 588, 590, 652, 656, 685, 692, 742, 749, 803(2), 820, 823, 855(2), 873(2), 1026, 1028, 1051, 1052, 1091, 1092, 1137, 1138, 1157, 1158, 1286(2), 1403, 1404, 1443, 1444, 1469, 1470, 1522(2), 3177, 3179, 3186, 3187, 3199, 3200, 3203, 3204, 3508, 3511
$K^+(C_4H_5N)_2$	0.28 (0.02)	5, 13, 86, 117, 124, 127, 146, 200, 546, 548, 577, 578, 644, 647, 667, 671, 726, 732, 786, 787, 800, 801, 853, 854, 872(2), 1030(2), 1053, 1054, 1092, 1093, 1141, 1142, 1158(2), 1288(2), 1411(2), 1449(2), 1474(2), 1528(2), 3175(2), 3184(2), 3197(2), 3201(2), 3515(2)
$Rb^+(C_4H_5N)_2$	0.28 (0.02)	5, 69, 90, 108, 110, 114, 140, 539, 540, 570(2), 640, 641, 659, 660, 720, 725, 779, 780, 791, 792, 852(2), 872(2), 1030, 1031, 1054(2), 1093(2), 1144(2), 1158(2), 1289(2), 1414(2), 1454, 1455, 1478(2), 1532(2), 3174(2), 3183(2), 3197(2), 3201(2), 3519(2)
$Cs^+(C_4H_5N)_2$	0.28 (0.02)	4, 63, 79, 103(2), 106, 118, 533, 534, 569(2), 636, 637, 654, 655, 716, 720, 776, 777, 789, 790, 852(2), 872(2), 1031(2), 1055(2), 1093(2), 1146(2), 1158(2), 1290(2), 1416(2), 1457(2), 1480(2), 1534(2), 3173(2), 3183(2), 3197(2), 3201(2), 3522(2)

[a] Obtained from vibrational analyses of the MP2(full)/6-31G* geometry optimized structures and scaled by 0.9646.
[b] Uncertainties are listed in parenthesis.
[c] Degeneracies are listed in parentheses.

reported below are in the center-of-mass frame unless otherwise noted. The absolute zero and distribution of the ion kinetic energies are determined using the octopole ion guide as a retarding potential analyzer as previously described [51]. The distribution of ion kinetic energies is nearly Gaussian with a fwhm between 0.2 and 0.4 eV (lab) for these experiments. The uncertainty in the absolute energy scale is ±0.05 eV (lab).

Pressure-dependent studies of all CID cross-sections examined here were performed because multiple collisions can influence the shape of CID cross-sections and the threshold regions are most sensitive to these effects. Data free from pressure effects are obtained by extrapolating to zero reactant pressure, as described previously [52]. Thus, cross-sections subjected to thermochemical analysis are the result of single bimolecular encounters.

2.2. Quantum chemical calculations

To obtain model structures, vibrational frequencies, and energetics for neutral pyrrole, C_4H_5N, and the $M^+(C_4H_5N)_x$ complexes, quantum chemical calculations were performed using Gaussian 98 and 03 [53]. Geometry optimizations and frequency analyses were performed at the MP2(full)/6-31G* level for $M^+(C_4H_5N)_x$ complexes where M = Li^+, Na^+, and K^+. For Rb^+ and Cs^+ complexes, geometry optimizations were performed using a hybrid basis set in which the effective core potentials (ECPs) and valence basis sets of Hay and Wadt were used to describe the metal cation [54], while the all-electron 6-31G* basis sets were used for C, N, and H atoms. The calculated vibrational frequencies were scaled by a factor of 0.9646 and are listed in Table 1. Table 2 lists the rotational constants for the ground state conformations. Single point energy calculations at the MP2(full)/6-311+G(2d,2p) and MP2(full)/Hybrid (6-311+G(2d,2p), Hay–Wadt) level of theory were performed using the MP2(full)/6-31G* and MP2(full)/Hybrid (6-31G*, Hay–Wadt) optimized geometries. To obtain accurate energetics, zero point energy (ZPE) and basis set superposition error (BSSE) corrections were included in the calculation of theoretical BDEs [55,56].

Table 2
Rotational constants of $M^+(C_4H_5N)_x$ and the corresponding PSL transition states for dissociation

Species	Energized molecule		Transition state		
	1-D[a]	2-D[b]	1-D[c]	2-D[c]	2-D[d]
$Na^+(C_4H_5N)$	0.151	0.107	0.152	0.303	0.0032
$K^+(C_4H_5N)$	0.151	0.066	0.152	0.303	0.0022
$Rb^+(C_4H_5N)$	0.151	0.040	0.152	0.303	0.0015
$Cs^+(C_4H_5N)$	0.151	0.030	0.152	0.303	0.0011
$Li^+(C_4H_5N)_2$	0.075	0.026	0.150, 0.152	0.209, 0.303	0.0022
$Na^+(C_4H_5N)_2$	0.075	0.019	0.151, 0.151	0.107, 0.303	0.0021
$K^+(C_4H_5N)_2$	0.073	0.015	0.151, 0.151	0.066, 0.303	0.0022
$Rb^+(C_4H_5N)_2$	0.073	0.015	0.151, 0.151	0.066, 0.303	0.0021
$Cs^+(C_4H_5N)_2$	0.073	0.015	0.151, 0.151	0.066, 0.303	0.0018

[a] Active external.
[b] Inactive external.
[c] Rotational constants of the transition state treated as free internal rotors.
[d] Treated variationally and statistically, value cited is obtained at the threshold energy for dissociation.

Polarizability is one of the key factors that influence the strength of cation-π interactions. To determine the influence of the polarizability on cation-π binding, the molecular polarizability of pyrrole was determined based on a dipole electric field and carried out using the PBE0 hybrid functional (also referred to as PBE1PBE) [57] and the 6-311+G(2d,2p) basis set. The PBE0 hybrid functional uses the generalized gradient approximation mixed with a predefined amount of Hartree–Fock exchange and provides polarizabilities that are in very good agreement with experimental values [58–60].

To more clearly visualize and better understand the influence of the N heteroaotom on cation-π binding, electrostatic potential maps of benzene, indole, and pyrrole were calculated, and NBO analyses of the pyrrole ligand and alkali metal cation–pyrrole complexes were carried out. The Natural Bond Orbital (NBO) program [61] in Gaussian performs an analysis of the many-electron molecular wave function in terms of localized electron-pair "bonding" units, and provides atomic charges, bond types, hybrid directions, resonance weights, bond orders, and other bonding parameters.

2.3. Thermochemical analysis

The threshold regions of the CID cross-sections are modeled using Eq. (1):

$$\sigma(E) = \sigma_0 \sum_i g_i (E + E_i - E_0)^n / E \quad (1)$$

where σ_0 is an energy independent scaling factor, E the relative translational energy of the reactants, E_0 the threshold for reaction of the ground electronic and ro-vibrational state, and n is an adjustable parameter that describes the efficiency of kinetic to internal energy transfer [62]. The summation is over the ro-vibrational states of the reactant ions, i, where E_i is the excitation energy of each ro-vibrational state and g_i is the population of those states ($\sum g_i = 1$).

The Beyer–Swinehart algorithm is used to evaluate the density of the ro-vibrational states [63–65], and the relative populations, g_i, are calculated as a Maxwell–Boltzmann distribution at 298 K, the internal temperature of the reactants. The average internal energies at 298 K of neutral pyrrole and the $M^+(C_4H_5N)_x$ complexes are also given in Table 1. We have estimated the sensitivity of our analysis to the deviations from the true frequencies by scaling the appropriately pre-scaled vibrational frequencies (0.9646) by ±10%. The corresponding change in the average vibrational energy is taken to be an estimate of one standard deviation of the uncertainty in vibrational energy (Table 1) and is included in the uncertainties listed with the E_0 and E_0(PSL) values.

We also consider the possibility that the collisionally activated complex ions do not dissociate on the time scale of the experiment ($\sim 10^{-4}$ s) by including statistical theories for unimolecular dissociation, specifically Rice-Ramsperger-Kassel-Marcus (RRKM) theory, into Eq. (1) as described in detail elsewhere [43,66]. The ro-vibrational frequencies appropriate for the energized molecules and the transition states (TSs) leading to dissociation are given in Tables 1S and 2S, where we assume that the TSs are loose and product-like because the interaction between the alkali metal cation and pyrrole ligand(s) is largely electrostatic. The TS vibrations used are the frequencies corresponding to the products, pyrrole and $M^+(C_4H_5N)_{x-1}$. The transitional frequencies, those that become rotations of the completely dissociated products, are treated as rotors corresponding to a phase space limit (PSL) as described in detail elsewhere [43].

The model represented by Eq. (1) is expected to be appropriate for translationally driven reactions [67] and has been shown to reproduce CID cross-sections well. The model of Eq. (1) is convoluted with the kinetic energy distributions of both reactants, and a nonlinear least-squares analysis of the data is performed to give optimized values for the parameters σ_0, E_0, and n. The errors associated with the measurement of E_0 and E_0(PSL) are estimated from the range of threshold values determined for the eight zero-pressure-extrapolated data sets, variations associated with uncertainties in the vibrational frequencies (scaled as described above), and the error in the absolute energy scale, 0.05 eV (lab). For analyses that include the RRKM lifetime analysis, the uncertainties in the reported E_0(PSL) values also include the effects of increasing and decreasing the time assumed available for dissociation ($\sim 10^{-4}$ s) by a factor of 2.

Eq. (1) explicitly includes the internal energy of the ion, E_i. All energy available is treated statistically because the ro-vibrational energy of the reactants is redistributed throughout the ion upon impact with Xe. Because the CID processes examined here are simple noncovalent bond cleavage reactions, the E_0 (PSL) values determined by analysis with Eq. (1) can be equated to 0 K BDEs [68,69].

3. Results

3.1. Cross-sections for collision-induced dissociation

Experimental cross-sections were obtained for the interaction of Xe with nine $M^+(C_4H_5N)_x$ complexes, where $M^+ = Na^+$, K^+, Rb^+, and Cs^+ for $x = 1$ and 2, and Li^+ for $x = 2$. Fig. 1 shows data for the $M^+(C_4H_5N)_x$ complexes. Over the collision energy range studied, two types of processes are observed: the sequential loss of intact pyrrole molecules and ligand exchange with Xe as summarized in reactions (2) and (3).

$$M^+(C_4H_5N)_x + Xe \rightarrow M^+(C_4H_5N)_{x-1} + C_4H_5N + Xe \quad (2)$$

$$\rightarrow XeM^+(C_4H_5N)_{x-1} + C_4H_5N \quad (3)$$

In all cases, the most favorable process is the loss of a single pyrrole molecule. Dissociation of a second pyrrole molecule is observed for the bis-complexes at elevated energies. The shape of the CID cross-sections confirm that these products are formed sequentially from the primary CID product, i.e., the intensity of primary $M^+(C_4H_5N)$ product begins to fall off as the secondary product, M^+, begins to appear. Ligand exchange to form M^+Xe is observed for the $M^+(C_4H_5N)$ complexes, where $M^+ = Na^+$, K^+, and Rb^+. It is likely that the analogous ligand exchange processes occurs for all complexes, but that the signal to noise

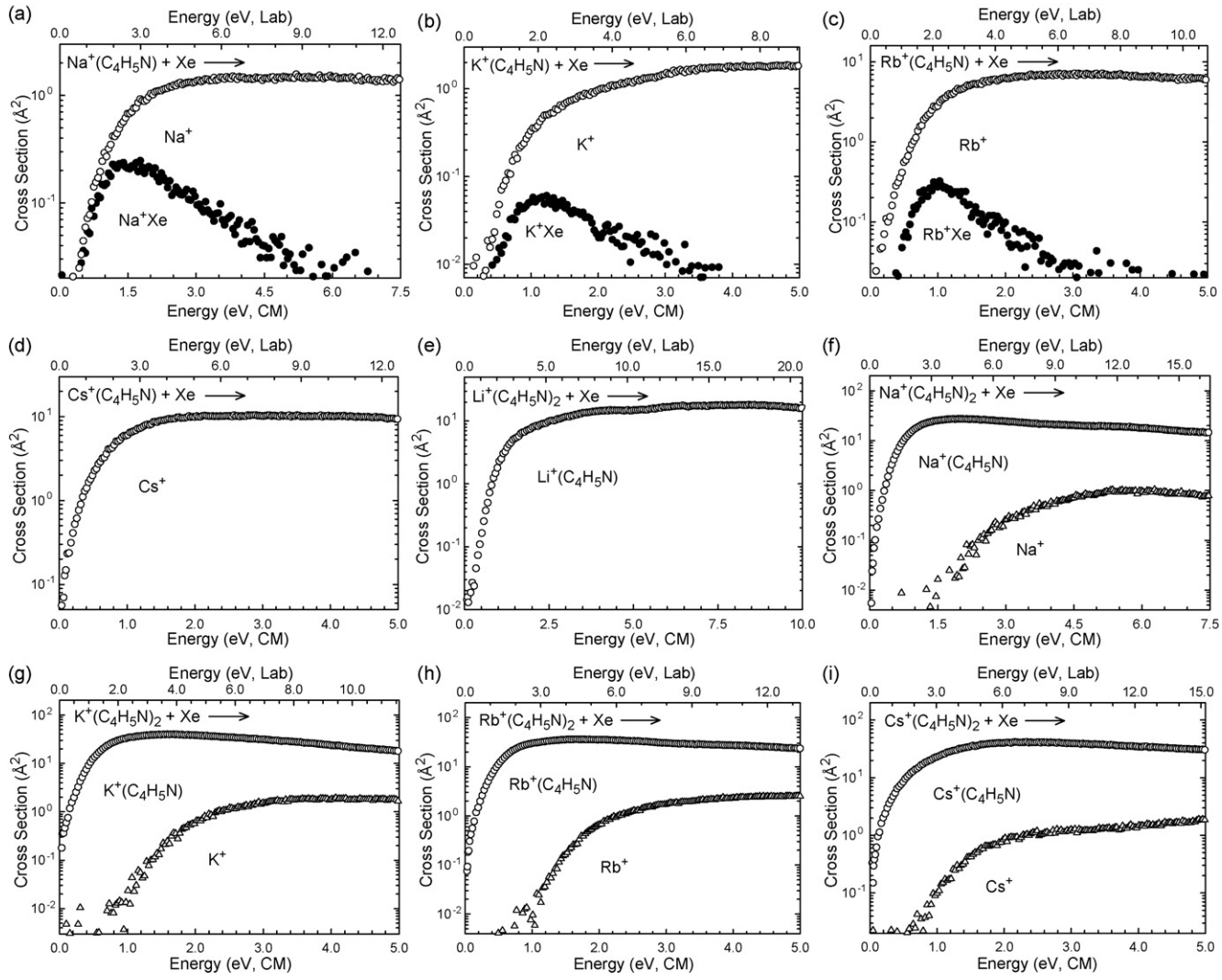

Fig. 1. (a–i) Cross-sections for the collision-induced dissociation of the $M^+(C_4H_5N)_x$ complexes, where $M^+ = Na^+$, K^+, Rb^+, and Cs^+ for $x = 1$ and 2, and Li^+ for $x = 2$, parts a through *i*, respectively, with Xe as a function of collision energy in the center-of-mass frame (lower *x*-axis) and laboratory frame (upper *x*-axis). Data for the primary CID product are shown for a Xe pressure of 0.2 mTorr.

in the other experiments was not sufficient to differentiate the M^+Xe and $XeM^+(C_4H_5N)$ products from background noise.

3.2. Threshold analysis

The model of Eq. (1) was used to analyze the thresholds for reactions (2) in nine $M^+(C_4H_5N)_x$ systems. The results of these analyses are provided in Table 3. Fitted results for the $M^+(C_4H_5N)_x$ complexes are shown in Fig. 2. In all cases, the experimental cross-sections for CID reactions (2) are accurately reproduced using a loose PSL TS model [43]. Previous work has shown that this model provides the most accurate assessment of the kinetic shifts for CID processes of electrostatically bound ion–molecule complexes [22,24–31,34,40,41,43,44]. Good reproduction of the data is obtained over energy ranges exceeding 1.5 eV and cross-section magnitudes of at least a factor of 100. Table 3 also lists values of E_0 obtained without including the RRKM lifetime analysis. Comparison of these values with the E_0(PSL) values shows that the kinetic shifts are larger for the bis-complexes than the corresponding mono-complexes as a result of the larger number of vibrational degrees of freedom, but are very small, 0 to 0.04 eV, for all systems.

The entropy of activation, $\Delta S^\dagger$, is a measure of the looseness of the TS and also a reflection of the complexity of the system. It is largely determined by the molecular parameters used to model the energized molecule and the TS for dissociation, but also depends on the threshold energy. The $\Delta S^\dagger$(PSL) values at 1000 K are listed in Table 3 and vary from 29 to 44 kJ/mol for the mono-complexes, and 34–67 J/K mol for the bis-complexes. The $\Delta S^\dagger$ values for the bis-complexes are larger than for the mono-complexes.

3.3. Theoretical results

Theoretical structures for neutral pyrrole and the $M^+(C_4H_5N)_x$ complexes were calculated as described above. Table 4 provides key geometrical parameters of the optimized

Table 3
Fitting parameters of Eq. (1), threshold dissociation energies at 0 K, and entropies of activation at 1000 K of $M^+(C_4H_5N)_x$

Species	σ_0[a]	n[a]	E_0 (eV)[b]	E_0 (PSL) (eV)	Kinetic shift (eV)	$\Delta S^\dagger$ (PSL) (J mol^{-1} K^{-1})
$Na^+(C_4H_5N)$	1.1 (0.1)	1.3 (0.1)	1.06 (0.08)	1.05 (0.08)	0.01	44 (3)
$K^+(C_4H_5N)$	1.2 (0.2)	1.4 (0.1)	0.81 (0.04)	0.81 (0.04)	0.00	39 (3)
$Rb^+(C_4H_5N)$	8.9 (2.6)	1.3 (0.2)	0.75 (0.06)	0.74 (0.06)	0.01	31 (3)
$Cs^+(C_4H_5N)$	10.1 (0.3)	1.3 (0.1)	0.53 (0.03)	0.52 (0.03)	0.01	29 (3)
$Li^+(C_4H_5N)_2$	20.2 (0.8)	1.5 (0.1)	1.16 (0.05)	1.14 (0.04)	0.02	67 (4)
$Na^+(C_4H_5N)_2$	34.3 (0.8)	1.1 (0.1)	0.92 (0.06)	0.90 (0.05)	0.02	48 (4)
$K^+(C_4H_5N)_2$	56.6 (1.6)	1.0 (0.1)	0.73 (0.05)	0.72 (0.03)	0.01	34 (5)
$Rb^+(C_4H_5N)_2$	42.4 (1.2)	1.0 (0.1)	0.71 (0.04)	0.69 (0.04)	0.02	34 (4)
$Cs^+(C_4H_5N)_2$	31.0 (1.0)	1.8 (0.1)	0.54 (0.04)	0.50 (0.03)	0.04	35 (4)

Uncertainties are listed in parentheses.
[a] Average values for loose PSL transition state.
[b] No RRKM analysis.

geometries for each of these species. The geometry-optimized structures for the $Na^+(C_4H_5N)_x$ complexes are shown in Fig. 3, while Cartesian coordinates of the geometry optimized structures for all species are given in Table 5.

Only one stable binding mode is found for the $M^+(C_4H_5N)$ complexes. The alkali metal cation binds to the π cloud of the pyrrole ligand and is displaced from the center of the ring in the direction away from the nitrogen atom, as might be expected

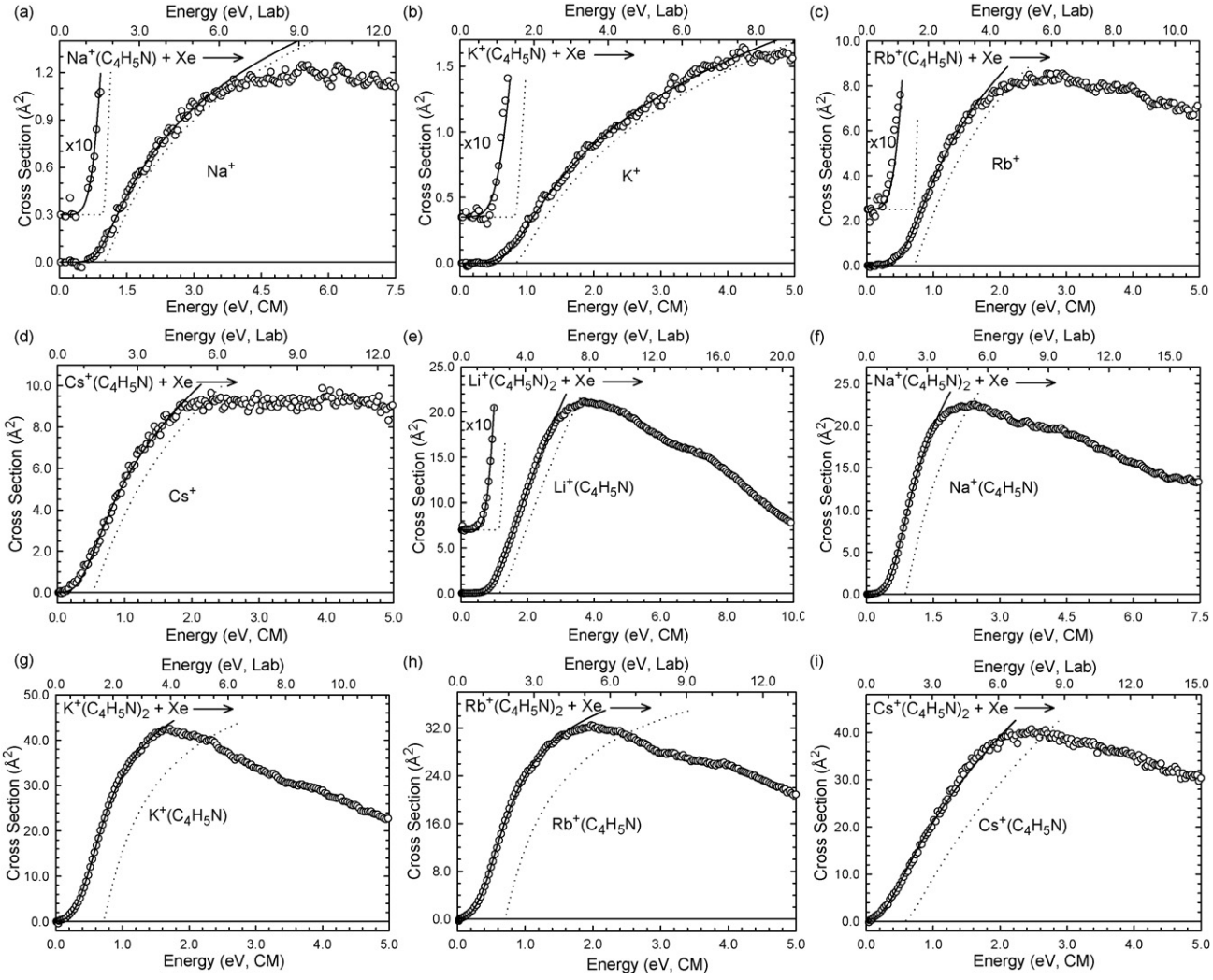

Fig. 2. (a–i) Zero-pressure-extrapolated cross-sections for collision-induced dissociation of the $M^+(C_4H_5N)_x$ complexes, where $M^+ = Na^+$, K^+, Rb^+, and Cs^+ for $x = 1$ and 2, and Li^+ for $x = 2$, parts a through *i*, respectively, with Xe in the threshold region as a function of kinetic energy in the center-of-mass frame (lower *x*-axis) and laboratory frame (upper *x*-axis). The solid lines show the best fits to the data using Eq. (1) convoluted over the neutral and ion kinetic and internal energy distributions. The dotted lines show the model cross-sections in the absence of experimental kinetic energy broadening for reactants with an internal energy corresponding to 0 K.

Table 4
Geometrical parameters of ground state MP2(full)/6-31G* optimized structures of pyrrole and $M^+(C_4H_5N)_x$ complexes

Species	Conformer	M^+–$R_\perp$ (Å)	M^+–R_C (Å)	Offset (Å)	C–C (Å)	C–H (Å)	CH OOP∠ (°)	N–H (Å)	NH OOP∠ (°)
C_4H_5N	–	–	–	–	1.417	1.082	0.00	1.011	0.00
$Li^+(C_4H_5N)$		1.940	1.959	0.269	1.425	1.083	1.96	1.018	6.88
$Na^+(C_4H_5N)$		2.414	2.416	0.101	1.425	1.083	3.44	1.016	7.92
$K^+(C_4H_5N)$		2.825	2.828	0.146	1.422	1.083	2.96	1.015	8.95
$Rb^+(C_4H_5N)$		3.104	3.104	0.062	1.422	1.083	3.02	1.015	8.73
$Cs^+(C_4H_5N)$		3.351	3.352	0.056	1.421	1.083	2.86	1.014	8.67
$Li^+(C_4H_5N)_2$	"*anti*"	1.979	1.993	0.233	1.424	1.082	2.22	1.016	4.60
	"*syn*"	1.981	1.998	0.264	1.423	1.082	1.38	1.016	7.24
$Na^+(C_4H_5N)_2$	"*anti*"	2.405	2.410	0.150	1.424	1.083	3.18	1.015	6.96
	"*syn*"	2.411	2.415	0.134	1.424	1.083	2.81	1.015	8.10
$K^+(C_4H_5N)_2$	"*anti*"	2.840	2.846	0.184	1.421	1.083	2.65	1.015	7.99
	"*syn*"	2.843	2.848	0.163	1.421	1.083	2.38	1.015	8.62
$Rb^+(C_4H_5N)_2$	"*anti*"	3.126	3.127	0.101	1.422	1.083	2.75	1.014	8.11
	"*syn*"	3.130	3.131	0.076	1.422	1.083	2.65	1.014	8.39
$Cs^+(C_4H_5N)_2$	"*anti*"	3.380	3.381	0.087	1.421	1.083	2.54	1.014	8.22
	"*syn*"	3.384	3.384	0.049	1.421	1.083	2.49	1.014	8.51

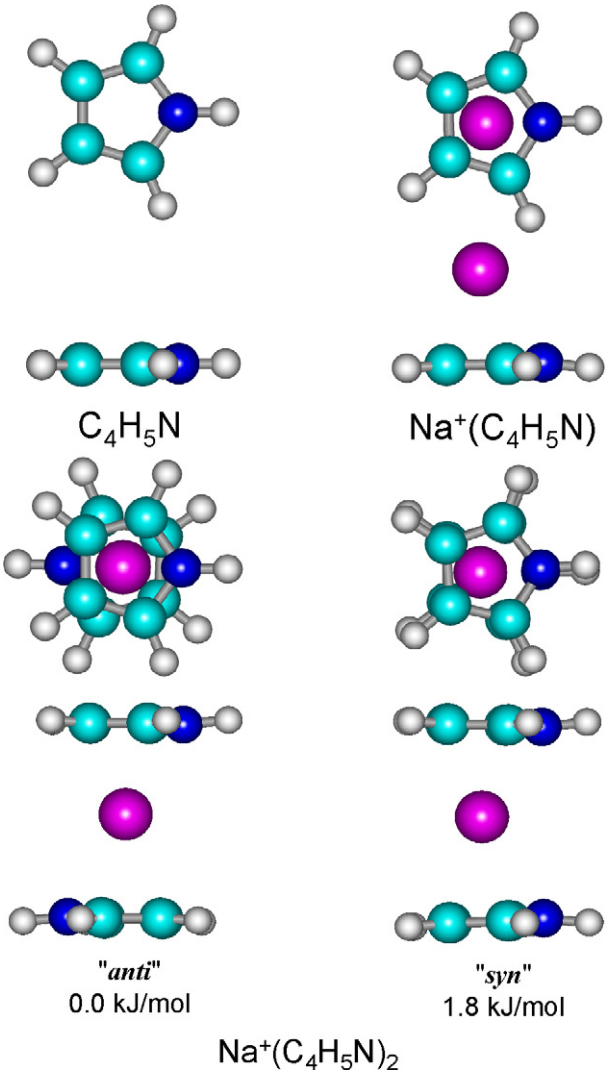

Fig. 3. MP2(full)/6-31G* optimized geometries of the $Na^+(C_4H_5N)$ and $Na^+(C_4H_5N)_2$ complexes. Two views of each structure are shown.

based on the dipole moment of the pyrrole ligand. The alkali metal cation–pyrrole ring distance (M^+–$R_\perp$) is found to increase from 1.940 to 3.351 Å as the size of alkali metal cation increases, while the strength of the cation-π interaction decreases from 158.1 to 57.0 kJ/mol.

Multiple stable binding modes are found for the $M^+(C_4H_5N)_2$ complexes in which the alkali metal cation binds to the π clouds and is sandwiched between the two pyrrole ligands. The only difference between these binding modes is the relative orientations of the pyrrole ligands. In the ground state conformations of the $M^+(C_4H_5N)_2$ complexes, the pyrrole ligands are aligned in an anti-parallel configuration such that their dipole moments nearly cancel; this geometry is designated the "*anti*" conformation. As found for the mono-complexes, the alkali metal cation–pyrrole ring distances (M^+–$R_\perp$) increase from 1.979 to 3.380 Å as the size of alkali metal cation increases, while the strength of the cation-π interaction decreases from 115.4 to 53.9 kJ/mol. An alternative binding mode is found for $M^+(C_4H_5N)_2$ complexes, in which the pyrrole ligands are aligned in a fanned-out parallel configuration, designated here as the "*syn*" conformation. The "*syn*" conformers are less stable than the "*anti*" conformers, but the differences in stability are less than 4.2 kJ/mol for all of the alkali metal cations. The small difference in the stability of these limiting conformations is significantly less than the average internal energy of these complexes at 298 K (see Table 1). Thus, it is reasonable to think of the $M^+(C_4H_5N)_2$ complexes accessed in our experiments as highly dynamic structures where the alkali metal cation interacts with both pyrrole rings with relative orientations that continuously vary between the "*anti*" and "*syn*" conformations.

The C–C bond lengths of the pyrrolyl ring increase by 0.004–0.008 Å upon complexation as compared to free pyrrole (Table 4). The change in the C–C bond lengths is largest for the Li^+ complex and decreases as the size of alkali metal cation increases. The C–H bond lengths are almost unaffected by complexation changing by at most 0.001 Å for all of the alkali metal

Table 5
MP2(full)/6-31G* optimized geometries of ground state pyrrole and $M^+(C_4H_5N)_x$

	C_4H_5N				$Li^+(C_4H_5N)$				$Na^+(C_4H_5N)$		
	x, *y*, *z*				*x*, *y*, *z*				*x*, *y*, *z*		
C	0.98148	0.71155	0.00000	C	0.33958	1.13412	-0.14879	C	0.64371	−1.13134	−0.22419
C	0.98608	−0.70539	0.00000	C	−0.98571	0.71267	−0.15348	C	0.30319	−0.70911	1.05466
C	−0.32988	−1.12544	−0.00000	C	−0.98560	−0.71279	−0.15349	C	0.30375	0.71625	1.04977
N	−1.11879	−0.00354	0.00000	C	0.33974	−1.13405	−0.14884	C	0.64459	1.12942	−0.23195
H	−2.12946	−0.00701	0.00002	N	1.12917	0.00009	−0.11380	N	0.82108	−0.00366	−0.99624
H	1.85344	−1.35167	0.00000	H	2.14187	0.00020	−0.21689	H	1.20251	−0.00704	−1.93789
H	−0.76371	−2.11530	−0.00001	H	0.77577	2.12359	−0.19354	H	0.81640	−2.12112	−0.62591
C	−0.33710	1.12342	−0.00000	H	−1.85162	1.36143	−0.19268	H	0.14268	−1.35537	1.90863
H	−0.77694	2.11061	−0.00001	H	−1.85142	−1.36168	−0.19274	H	0.14371	1.36849	1.89927
H	1.84473	1.36323	0.00000	H	0.77606	−2.12346	−0.19365	H	0.81799	2.11630	−0.64048
				Li	−0.04765	−0.00012	1.80460	Na	−1.84021	−0.00064	−0.31998

	$K^+(C_4H_5N)$				$Rb^+(C_4H_5N)$				$Cs^+(C_4H_5N)$		
	x, *y*, *z*				*x*, *y*, *z*				*x*, *y*, *z*		
C	1.00648	−0.30494	1.12843	C	1.61216	−0.30399	1.12859	C	2.06332	−0.30907	1.12803
C	0.88813	1.01186	0.71132	C	1.47970	1.01194	0.71123	C	1.94521	1.00748	0.71077
C	0.88822	1.01263	−0.71018	C	1.47971	1.01217	−0.71091	C	1.94522	1.00766	−0.71050
C	1.00663	−0.30370	−1.12872	C	1.66994	−1.08963	−0.00017	C	2.06334	−0.30877	−1.12811
N	1.05416	−1.09113	−0.00057	N	1.91269	−2.07475	−0.00032	N	2.11268	−1.09537	−0.00014
H	1.29028	−2.07850	−0.00110	H	1.91269	−2.07475	−0.00032	H	2.34629	−2.08229	−0.00027
H	1.11421	−0.73287	2.11631	H	1.72291	−0.73075	2.11672	H	2.16687	−0.73736	2.11619
H	0.86632	1.87781	1.36106	H	1.44965	1.87798	1.36085	H	1.92066	1.87357	1.36042
H	0.86649	1.87930	−1.35898	H	1.44967	1.87840	−1.36026	H	1.92068	1.87393	−1.35992
H	1.11447	−0.73056	−2.11705	H	1.72294	−0.73009	−2.11694	H	2.16692	−0.73680	−2.11638
K	−1.86145	−0.05644	−0.00007	Rb	1.61216	−0.30399	1.12859	Cs	−1.33478	−0.01650	−0.00000

	$Li^+(C_4H_5N)_2$				$Na^+(C_4H_5N)_2$				$K^+(C_4H_5N)_2$		
	x, *y*, *z*				*x*, *y*, *z*				*x*, *y*, *z*		
C	2.00438	−0.27476	−1.14321	C	2.45016	−0.31739	−1.12543	C	−2.87162	0.31662	−1.12511
C	1.94092	1.03253	−0.67665	C	2.34046	1.00712	−0.72390	C	−2.85589	−0.99445	−0.67526
C	1.94525	0.98204	0.74662	C	2.33881	1.02458	0.70000	C	−2.82990	−0.95965	0.74499
C	2.01135	−0.35488	1.11897	C	2.44686	−0.29020	1.13360	C	−2.83043	0.37187	1.13041
N	2.02054	−1.10113	−0.04006	N	2.48920	−1.09041	0.01372	N	−2.83555	1.13164	−0.01690
H	2.13991	−2.10974	−0.07616	H	2.68279	−2.08702	0.02599	H	−2.97412	2.13665	−0.03900
H	2.05818	−0.67363	−2.14718	H	2.54234	−0.75942	−2.10843	H	−2.95580	0.72751	−2.12231
H	1.93928	1.92086	−1.29510	H	2.32887	1.86527	−1.38407	H	−2.91243	−1.87514	−1.30249
H	1.94667	1.82428	1.42648	H	2.32560	1.89859	1.33901	H	−2.86310	−1.80856	1.41617
H	2.06972	−0.82387	2.09189	H	2.53621	−0.70883	2.12705	H	−2.87837	0.83111	2.10874
C	−1.94139	−1.03181	−0.67765	C	−2.34316	−1.03311	−0.68505	C	2.76928	0.95331	−0.79368
C	−2.01119	0.35390	1.11928	C	−2.44746	0.33604	1.12141	C	2.85700	−0.18143	1.16396
C	−2.00425	0.27598	−1.14292	C	−2.44871	0.27501	−1.13747	C	2.90517	−0.39575	−1.08185
H	−1.94028	−1.91954	−1.29697	H	−2.33413	−1.91619	−1.31117	H	2.75043	1.75301	−1.52330
H	−2.06947	0.82192	2.09267	H	−2.53635	0.79342	2.09779	H	2.94054	−0.51330	2.19023
H	−2.05786	0.67588	−2.14648	H	−2.53879	0.67997	−2.13658	H	3.03115	−0.91492	−2.02257
C	−1.94569	−0.98271	0.74566	C	−2.34243	−0.99451	0.73902	C	2.73891	1.08826	0.62047
H	−1.94762	−1.82560	1.42471	H	−2.33244	−1.84248	0.41194	H	2.69230	2.01150	1.18410
N	−2.02009	1.10126	−0.03900	N	−2.48607	1.09149	−0.02887	N	2.93652	−1.07080	0.11688
H	−2.13859	2.11001	−0.07412	H	−2.67621	2.08872	−0.05566	H	3.16506	−2.05456	0.21570
Li	0.00028	−0.00108	0.00435	Na	0.00119	−0.00590	−0.00300	K	0.00013	−0.10063	−0.03730

	$Rb^+(C_4H_5N)_2$				$Cs^+(C_4H_5N)_2$		
	x, *y*, *z*				*x*, *y*, *z*		
C	−0.60612	−0.89350	3.19625	C	3.40895	0.34691	−1.12998
C	0.76836	−0.71290	3.16236	C	3.35077	−0.96942	−0.70008
C	1.01472	0.68527	3.08727	N	3.42293	1.14522	−0.00963
C	−0.21508	1.32600	3.07703	H	−0.00005	−0.05725	−0.00112
N	−1.18637	0.35228	3.12416	Cs	3.34951	−0.95591	0.72078
H	−2.17405	0.53395	3.26630	C	3.40694	0.36836	1.12568

Table 5 (*Continued*)

	$Rb^+(C_4H_5N)_2$				$Cs^+(C_4H_5N)_2$		
	x, *y*, *z*				*x*, *y*, *z*		
H	−1.20533	−1.78656	3.31448	C	3.60208	2.14312	−0.01896
H	1.50840	−1.49967	3.23993	H	3.36204	−1.84185	−1.34144
H	1.97993	1.17617	3.09686	H	3.35961	−1.81597	1.37865
H	−0.47177	2.37695	3.09161	H	3.48528	0.81054	2.10996
C	−1.03964	−0.73283	−3.02808	H	−3.42946	−0.27769	−1.12455
C	0.44781	0.96693	−3.20021	C	−3.29010	1.03979	−0.71743
C	0.23098	−1.27847	−3.13197	C	−3.49191	−1.05414	0.00941
H	−1.96393	−1.29536	−2.98376	N	−3.53620	−0.71242	−2.10948
H	0.96934	1.90594	−3.33007	H	−3.28880	1.05076	0.70346
H	0.56217	−2.30611	−3.20164	C	−3.42739	−0.26028	1.13113
C	−0.90305	0.68162	−3.07109	C	−3.73225	−2.03910	0.01723
H	−1.70255	1.41201	−3.06666	H	−3.24827	1.90002	−1.37383
N	1.12179	−0.23287	−3.21588	H	−3.24574	1.92101	1.34643
H	2.10635	−0.33449	−3.43742	H	−3.53228	−0.67975	2.12285
Rb	0.07177	−0.03437	0.00279	H	−3.28880	1.05076	0.70346

Obtained from structures optimized at the MP2(full)/6-31G* level of theory.

cations. The N–H bond lengths increase by 0.003–0.007 Å upon complexation, with the largest increase in bond lengths for the smallest alkali metal cations. The change of bond lengths is larger for the mono-complexes than for the bis-complexes as a result of the increased separation of the alkali metal cation and pyrrole ligands in the latter complexes. The largest effect of the alkali metal cation on the pyrrole ring is the bending of the hydrogen atoms out of the plane and away from the alkali metal cation (CH and NH OOP∠s). The magnitude of CH OOP ∠s are smaller than the corresponding NH OOP ∠s for both mono- and bis-complexes of all of the alkali metal cations. The bending for the mono-complexes is larger than for the corresponding "*anti*" conformer of the bis-complex for all of the alkali metal cations. The magnitude of the bending is smaller for the complex to Li^+ than the other alkali metal cations. For the CH OOP∠s, the bending is larger for the "*anti*" conformers than the "*syn*" conformers. For the NH OOP∠s, however, the bending is smaller for the "*anti*" conformers than the "*syn*" conformers. The M^+–R_c and M^+–$R_\perp$ distances are found to increase as the size of alkali metal cation increases, as a result of the electrostatic binding in these complexes. These distances are also found to increase from the mono- to the corresponding bis-complex as a result of repulsive forces between the two pyrrole ligands. Both the M^+–R_c and M^+–$R_\perp$ distance are larger for the "*syn*" conformers than those for the corresponding "*anti*" conformers because of the larger ligand–ligand repulsion, and therefore weaker binding, arising from repulsive dipole–dipole interactions.

4. Discussion

4.1. Trends in the binding of alkali metal cations to pyrrole

The 0 K experimental BDEs of the $M^+(C_4H_5N)_x$ complexes are summarized in Table 6. The variation in the measured BDEs with the size of the alkali metal cation is shown in Fig. 4. The M^+–(C_4H_5N) and $(C_4H_5N)M^+$–(C_4H_5N) BDEs are found to decrease monotonically as the size of alkali metal cation increases from Li^+ to Cs^+. This can be explained in terms of the electrostatic interactions. The alkali metal cations have s^0 electron configurations and spherically symmetric electron densities. The alkali metal cation–ligand bond lengths are mainly determined by the size of the cation, such that the larger the cation radius the longer the bond distance, and the weaker the interaction. This trend is similar to that observed for the analogous alkali metal cation–aromatic ligand interactions previously studied [22,24–31,34] and supports the conclusion that these interactions are electrostatic in nature.

The BDEs of the bis-complexes are smaller than the corresponding mono-complexes as a result of ligand–ligand repulsive forces. The difference in the binding energy between the first and the second ligands is largest for Li^+ and decreases with the size of the alkali metal cation from 67.0 to 14.5 to 8.8 to 4.6 to 2.0 kJ/mol for the Li^+, Na^+, K^+, Rb^+, and Cs^+ complexes, respectively. The fall off in the sequential BDEs is more rapid than found for the corresponding complexes to benzene and arises from the greater Coulombic and dipole–dipole repulsions between the two pyrrole ligands. The distance between the two pyrrole ligands increases with the size of alkali metal cation from 3.986 Å in $Li^+(C_4H_5N)_2$ to 6.762 Å in $Cs^+(C_4H_5N)_2$ (Table 4; 2× M^+–Rc). The magnitude of the ligand–ligand repulsive forces decreases with increasing separation of the two pyrrole ligands, resulting in smaller differences in the sequential BDEs as the size of the alkali metal cation increases.

4.2. Comparison of theory and experiment

The $M^+(C_4H_5N)_x$ BDEs at 0K were calculated at the MP2(full)/6-311+G(2d,2p)//MP2(full)/6-31G* level of theory including ZPE and BSSE corrections. The experimental and theoretical BDEs of the $M^+(C_4H_5N)_x$ complexes are summarized in Table 6. The agreement between theory and experiment is illustrated in Fig. 5. Good agreement between the theoretical and the TCID experimental results is obtained for all complexes examined here. The mean absolute deviation (MAD) for all nine complexes is 3.7 ± 2.3 kJ/mol, slightly smaller than

Table 6
Enthalpies of alkali metal cation binding to pyrrole, benzene, and indole at 0 K in kJ/mol

Complex	Experiment (TCID)[a]			Conformer	Theory (L = C_4H_5N)			Literature
	C_4H_5N[b]	C_6H_6[c]	C_8H_7N[d]		D_e[e]	D_0[e,f]	$D_{0,BSSE}$[e,g]	
$Li^+(L)$	177.4 (16.6)[h]	161.1 (13.5)	204.5 (8.7)		175.1	167.3	158.1	
$Na^+(L)$	101.3 (7.7)	92.6 (5.8)	121.1 (2.9)		115.7	111.1	102.0	
	101.8 (2.9)[h]							107.9[j]
$K^+(L)$	78.5 (3.9)	73.3 (3.8)	99.8 (3.9)		89.6	85.9	80.7	
	83.7 (3.9)[h]							
$Rb^+(L)$[i]	71.4 (6.8)	68.5 (3.8)	90.1 (2.9)		74.0	71.1	64.7	
$Cs^+(L)$[i]	50.4 (2.9)	64.6 (4.8)	82.3 (2.9)		65.4	62.7	57.0	
$Li^+(L)_2$	110.4 (3.9)	104.2 (6.8)	119.6 (4.8)	"*anti*"	138.9	133.5	115.4	
				"*syn*"	134.5	129.2	111.2	
$Na^+(L)_2$	86.8 (4.8)	80.0 (5.8)	97.4 (2.9)	"*anti*"	102.3	98.2	84.1	82.0[j]
				"*syn*"	100.4	96.4	82.3	
$K^+(L)_2$	69.7 (3.9)	67.5 (6.8)	76.2 (2.9)	"*anti*"	80.1	77.0	68.3	
				"*syn*"	79.1	76.1	67.5	
$Rb^+(L)_2$[i]	66.8 (3.9)	62.7 (7.7)	73.3 (2.9)	"*anti*"	75.7	73.1	64.1	
				"*syn*"	73.8	71.4	62.8	
$Cs^+(L)_2$[i]	48.4 (2.9)	58.8 (7.7)	68.5 (2.9)	"*anti*"	63.8	61.5	53.9	
				"*syn*"	63.1	61.9	53.4	

[a] Threshold collision-induced dissociation. Uncertainties are listed in parentheses.
[b] Present results. Uncertainties are listed in parenthesis.
[c] Ref. [30].
[d] Ref. [34].
[e] Calculated at the MP2(full)/6-31G*//MP2(full)/6-311+G(2d,2p), present results.
[f] Including ZPE corrections with MP2(full)/6-31G* frequencies scaled by 0.9646.
[g] Also includes BSSE corrections.
[h] Ref. [31].
[i] The Hay–Wadt ECP/valence basis set was used for the metal cation, as described in the text, and the 6-31G* and 6-311+G(2d,2p) basis set were used for C, N, and H in geometry optimizations and single point calculations, respectively.
[j] B3LYP, including ZPE and BSSE corrections, Ref. [32].

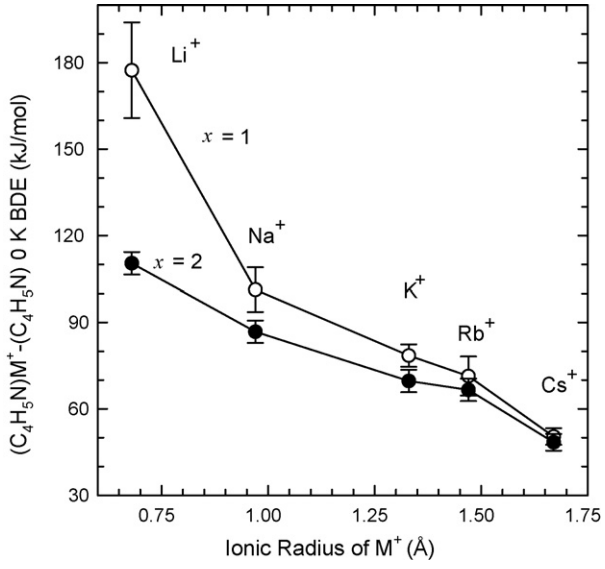

Fig. 4. Bond dissociation energies at 0 K (kJ/mol) of the $M^+(C_4H_5N)_x$ complexes plotted vs. the ionic radius of M^+. Data are shown for $x = 1$ and 2 as ○ and ●, respectively. All values are measured by TCID and taken from Table 2. The BDE of $Li^+(C_4H_5N)$ is taken from Ref. [31].

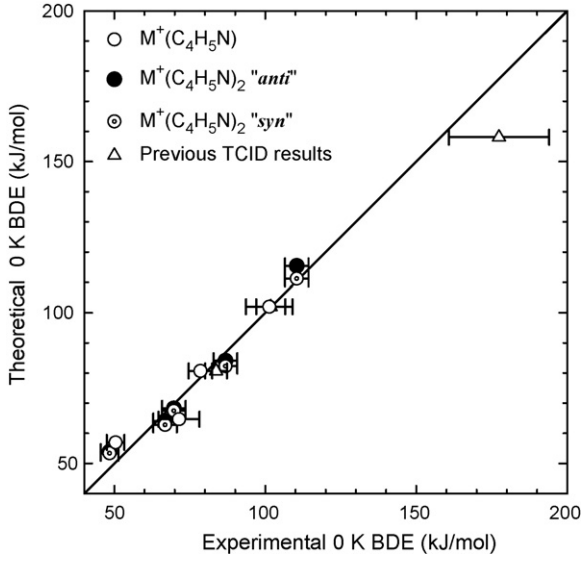

Fig. 5. Theoretical vs. experimental 0 K bond dissociation energies of M^+–(C_4H_5N) and (C_4H_5N)M^+–(C_4H_5N) (kJ/mol), where $M^+ = Li^+$, Na^+, K^+, Rb^+, and Cs^+.

the average experimental uncertainty (AEU), 4.5 ± 1.7 kJ/mol, and well within the 8 kJ/mol expected accuracy of this level of theory [22]. For the mono-complexes, the measured MAD is 4.1 ± 3.1 kJ/mol, smaller than the AEU, 5.3 ± 2.3 kJ/mol. Theory systematically underestimates the BDE of the $Li^+(C_4H_5N)$ [31] complex because the basis sets employed in the current study do not allow core correlation, and the higher degree of covalency in the Li^+–pyrrole interactions requires such core correlation to accurately describe the interaction. The higher degree of covalency is also indicated by the partial charge on M^+, which is 0.81e for Li^+ and 0.91e–0.98e for all other alkali metal cations. An independent study of Li^+(ligand) complexes has been conducted to determine the level of theory necessary to achieve an accurate description of the binding in Li^+ systems [70]. In this work it is found that G3 and complete basis set (CBS) extrapolation of calculations performed at the MP2(full)/aug-cc-PVnZ//MP2(full)/cc-PVDZ levels of theory where n = D, T, and Q and additional core correlation functions have been added to Li^+ to provide the most accurate bond energies of Li^+(ligand) complexes. The G3 and CBS BDEs for Li^+(pyrrole) were calculated to be 167.6 and 164.8 kJ/mol, respectively. Both of these values are in much better agreement with the previously measured BDE for the Li^+(pyrrole) complex of 177.4 ± 16.6 kJ/mol than the MP2 value including BSSE corrections computed here, 158.1 kJ/mol. It is interesting to note, that the G3 and CBS values are similar to the value calculated here when BSSE corrections are not included, 167.3 kJ/mol. In an earlier study of the binding of alkali metal cations to benzene, Feller, Dixon, and Nicholas estimated the binding enthalpies of these complexes in the complete basis set (CBS) limit from calculations performed with three members of the diffuse function augmented correlation-consistent family of basis sets (i.e., aug-cc-pVxZ, x = D, T, and Q). They found that the CBS values were closer to the raw binding energies than those corrected for BSSE. This behavior is consistent with the values for the Li^+(pyrrole) complex found here and for a number of noncovalently bound metal–ligand complexes previously studied both experimentally and theoretically [71]. For the bis-complexes, the measured BDEs are in good agreement with calculated values for all of the alkali metal cations. The MADs between the experimental and theoretical BDEs are 3.4 ± 1.6 and 3.3 ± 1.8 kJ/mol for the "*anti*" and "*syn*" conformers, respectively, slightly smaller than the AEU of these systems, 3.9 ± 0.7 kJ/mol. Because our threshold measurements provide the BDE for the most weakly bound species present in reasonable abundance, it is probably most appropriate to compare the measured BDEs with those calculated for the "*syn*" conformers.

4.3. Conversion from 0 to 298 K

The 0 K BDEs determined here are converted to 298 K bond enthalpies and free energies to allow comparison to literature values and commonly employed experimental conditions. The conversions are calculated using standard formulas (assuming harmonic oscillator and rigid rotor models) and the vibrational and rotational constants determined for the MP2(full)/6-31G* optimized geometries, listed in Tables 1 and 2. Table 7 lists the 0 and 298 K enthalpy, free energy, and enthalpic and entropic corrections for all $M^+(C_4H_5N)_x$ complexes experimentally and theoretically determined (from Table 6). Uncertainties are determined by 10% variation in the molecular constants.

4.4. Influence of the N heteroatom on cation-π binding

The N heteroatom of pyrrole and indole shares one pair of electrons with the aromatic ring, i.e., 6 π electrons over 5 atoms for pyrrole and 10 π electrons over 9 atoms for indole. The π electron density is therefore 1.2 and 1.1 per ring atom for pyrrole and indole, respectively. From this simple analysis, it is clear that pyrrole and indole are π excessive as compared to

Table 7
Enthalpies and free energies of binding of $M^+(C_4H_5N)_x$ at 298K in kJ/mol[a]

System	ΔH_0	ΔH_0[b]	$\Delta H_{298}-\Delta H_0$[b]	ΔH_{298}	ΔH_{298}[b]	$T\Delta S_{298}$[b]	ΔG_{298}	ΔG_{298}[b]
$Na^+(C_4H_5N)$	101.3 (7.7)	102.0	1.8 (0.2)	103.1 (7.7)	103.8	31.5 (0.6)	71.6 (7.7)	72.3
$K^+(C_4H_5N)$	78.5 (3.9)	80.7	1.4 (0.2)	79.9 (3.9)	82.1	30.5 (0.6)	49.4 (3.9)	32.7
$Rb^+(C_4H_5N)$	71.4 (6.8)	61.2	0.9 (0.1)	72.3 (6.8)	62.1	28.9 (0.7)	43.4 (6.8)	33.2
$Cs^+(C_4H_5N)$	50.4 (2.9)	53.6	0.7 (0.1)	51.1 (2.9)	54.3	28.1 (0.7)	23.0 (3.0)	26.2
$Li^+(C_4H_5N)_2$	110.4 (3.9)	115.4	−1.1 (0.7)	109.3 (3.9)	114.3	40.6 (1.2)	68.7 (4.1)	73.7
		111.2	−0.2 (0.2)	110.2 (3.9)	111.0	43.0 (1.1)	67.2 (4.1)	68.0
$Na^+(C_4H_5N)_2$	86.8 (4.8)	84.1	−0.8 (0.2)	86.0 (4.8)	83.3	37.7 (1.1)	48.3 (4.8)	45.6
		82.3	−0.8 (0.2)	86.0 (4.8)	81.5	38.4 (1.1)	47.6 (4.8)	43.1
$K^+(C_4H_5N)_2$	69.7 (3.9)	68.3	−1.2 (0.2)	68.5 (3.9)	67.1	33.9 (1.2)	34.6 (4.1)	33.2
		67.5	1.1 (0.2)	70.8 (3.9)	68.6	41.3 (0.7)	29.5 (4.1)	27.3
$Rb^+(C_4H_5N)_2$	66.8 (3.9)	64.1	−1.2 (0.2)	65.6 (3.9)	62.9	33.9 (1.2)	31.7 (4.1)	29.0
		62.8	1.1 (0.2)	67.9 (3.9)	63.9	41.3 (0.7)	26.6 (4.1)	22.6
$Cs^+(C_4H_5N)_2$	48.4 (2.9)	53.6	−1.2 (0.2)	47.2 (2.9)	52.4	33.9 (1.2)	13.3 (3.1)	18.5
		53.4	1.1 (0.2)	49.5 (2.9)	54.5	41.3 (0.7)	8.2 (3.1)	13.2

[a] Uncertainties are listed in the parentheses.
[b] Ab initio values from theoretical calculations at the MP2(full)/6-311+G(2d,2p) level of theory using the MP2(full)/6-31G* optimized geometries with frequencies scaled by 0.9646. Uncertainties in the enthalpic and entropic corrections are determined by 10% variation in the molecular constants.

benzene, which has 6 π electrons distributed over 6 atoms resulting in a π electron density of 1.0. Thus, the measured BDEs of the $M^+(C_4H_5N)_x$ complexes are expected to be greater than those of the corresponding $M^+(C_6H_6)_x$ [30] complexes. This is exactly what is observed for all of the alkali metal cations except Cs^+. Similarly, the calculated BDEs of $M^+(C_4H_5N)_x$ are greater than $M^+(C_6H_6)_x$ for all of the alkali metal cations (Table 2). However, in the $M^+(C_8H_7N)$ complexes, all of the alkali metal cations favor binding to the π cloud above the phenyl ring over the pyrrolyl ring of the indole ligand, which cannot be explained by this simple π character analysis. In this study, the electrostatic potential maps of the isolated ligands and NBO analyses of these complexes are used to examine the influence of the N heteroatom on the distribution of electron density and binding geometry of the N containing ligands in detail. The natural charge populations and electrostatic potential maps of the Na^+ complexes are showed in Figs. 6 and 7, respectively. The negative charge is evenly distributed over the carbon atoms of benzene and produces a symmetric electrostatic potential map. Thus, alkali metal cations bind to the center of π cloud of benzene. However, the lone pair of electrons of N delocalize electron density to C2 (−0.327e) and C3 (−0.327e) of pyrrole and to C5 (−0.264e), C7 (−0.270e) and C3 (−0.324e) of indole and thus produces asymmetric electrostatic potential surfaces for these ligands. Therefore, alkali metal cations bind to the π cloud of pyrrole close to the C2–C3 bond. Because positive charge is concentrated on C8 (0.190e) and C2 (0.023e) of indole, the alkali metal cations prefer to bind near C5 and C3 of indole corresponding to the phenyl and pyrrolyl rings, respectively. Furthermore, redistribution of electron density is found after alkali metal binding to indole. For the π6 conformer, all of the carbon atoms become more negative than in the free ligand as a result of greater degree of electron density delocalization from N and H into the ring. While for the π5 comformer, C2, C3, C4, C8, C9, and N1 become more negative while C5, C6, and C7 become more positive as a result of electron density

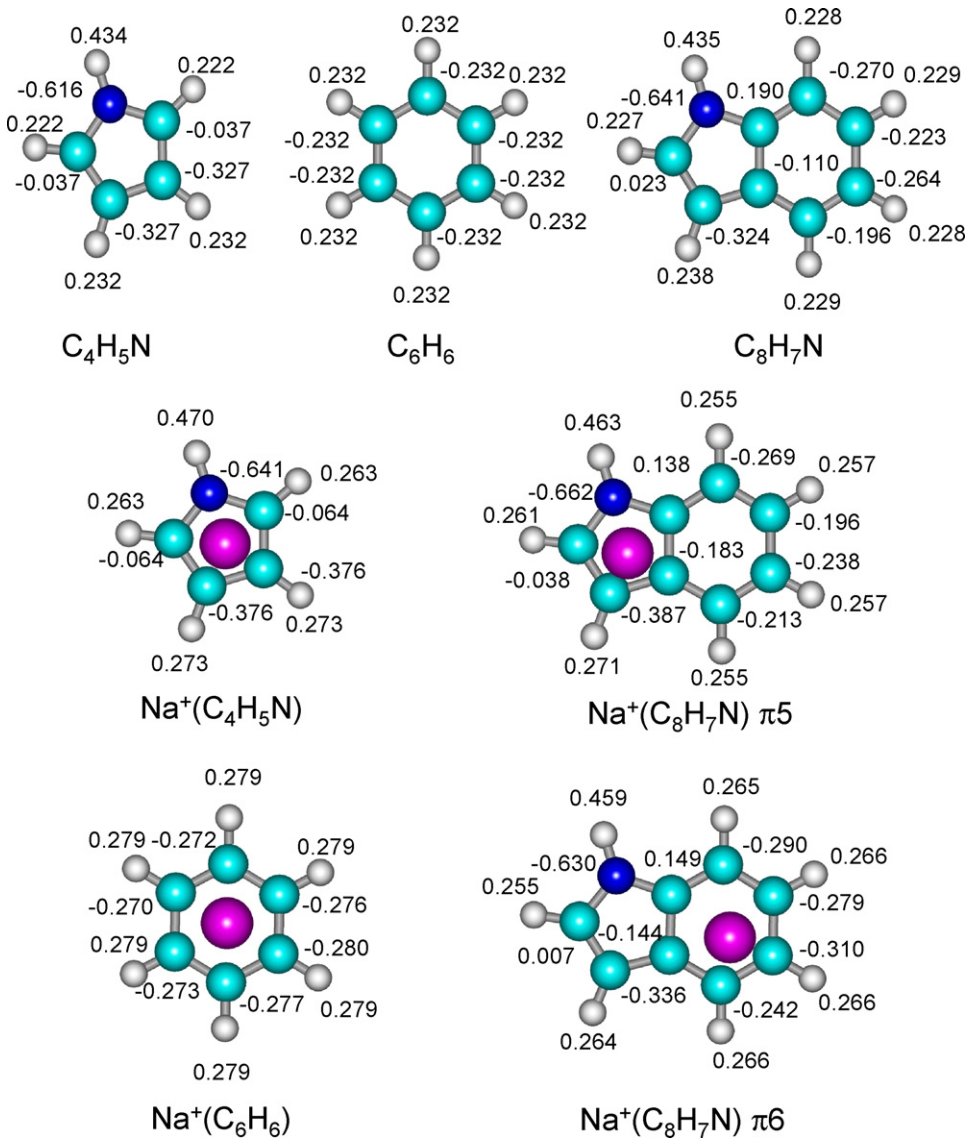

Fig. 6. Natural charges of neutral pyrrole, benzene, and indole and their complexes to Na^+.

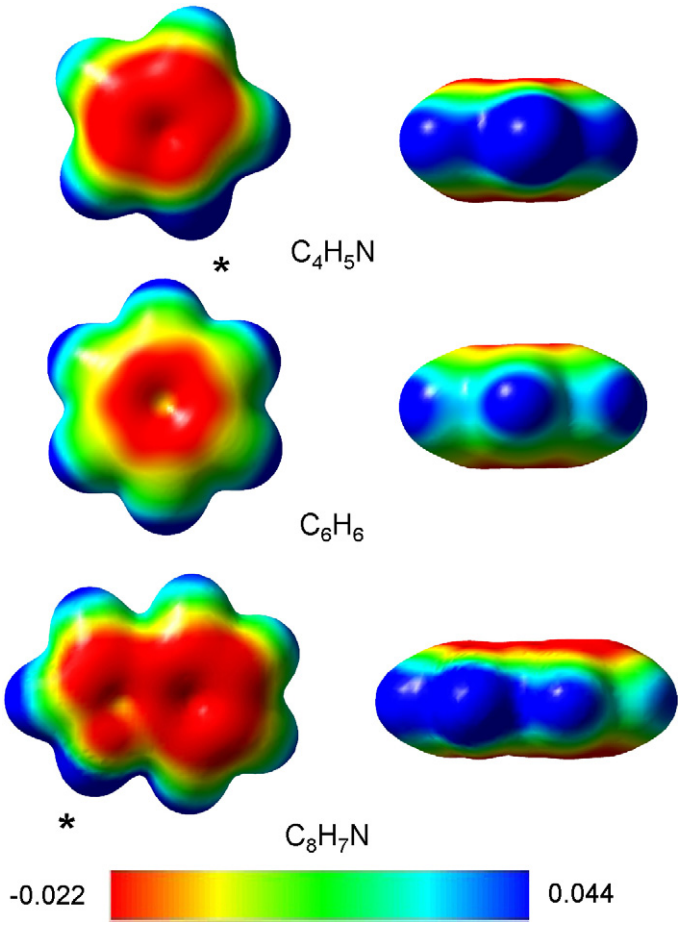

Fig. 7. Electrostatic potential maps of pyrrole, benzene, and indole at an isosurface of 0.05 au of the total SCF electron density. The position of the ring N atom of pyrrole and indole are indicated with an asterisk. Top and side views are shown, respectively.

withdrawal from the 6-membered ring, which thereby enhances the binding to the pyrrolyl site. Our calculations show that the differences in BDEs between the phenyl and pyrrolyl rings of indole account for only ~10% of the corresponding total BDE of the ground state conformers for all five alkali metal cations. Gokel and co-workers found that metal cations can be stabilized by interaction with the pyrrolyl ring [38,39]. Thus, their results along with the theoretical results indicate that the π clouds of the pyrrolyl and phenyl rings of indole cooperate with each other, such that the whole π surface of indole is favorable for cation-π binding. This suggests that indole may maintain significant stabilization via cation-π interaction even when optimum binding is not possible due to steric interactions or slight geometrical changes that may occur in proteins and enzymes during biological processes. The ability of the indolyl side chain of Trp to provide relatively strong binding of cations over the entire π surface may well explain the preference of Trp for engaging in cation-π interactions in nature.

The relative binding affinities of benzene, pyrrole, and indole to alkali metal cations can be understood by examining the dipole moment, quadrupole moment, and polarizability of these ligands. Benzene has a center of symmetry and thus has no dipole moment. The N heteroatom of pyrrole and indole leads to a dipole moment that points towards the π ring and lies in the plane of the π surface, and thus ion–dipole interactions do not contribute directly to the binding. However, electron density from the electron-rich N heteroatom is partially delocalized into the π cloud along the direction of the dipole moment. The π-excessive character of pyrrole and indole leads to an increase in the quadrupole moments of pyrrole and indole as compared to benzene. Thus only ion–quadrupole and ion-induced dipole interactions play a direct role in the binding in the $M^+(C_4H_5N)_x$ and $M^+(C_8H_7N)_x$ complexes. The polarizabilities of pyrrole, benzene, and indole are calculated to be 7.82, 10.00, and 14.87 $Å^3$, respectively [33]. Therefore, the ion-induced dipole interaction should result in stronger binding to benzene and even stronger binding to indole as compared to pyrrole. However, this trend is not consistent with the measured or calculated BDEs for these systems indicating that the ion-induced dipole interactions do not dominate the binding. According to NBO analyses and electrostatic potential maps, pyrrole and indole are π-excessive ligands as compared to benzene such that ion–quadrupole interactions to pyrrole are stronger than benzene and weaker than indole. This trend parallels the measured and calculated BDEs for the alkali metal cation complexes of benzene, pyrrole, and indole. This behavior indicates that the ion–quadrupole interaction dominates the cation-π interaction in alkali metal cation complexes to benzene, pyrrole, and indole, as has been concluded for other aromatic ligands previously studied [22,24–30]. It is also clear that the N atom enhances cation-π binding to pyrrole and indole because it delocalizes part of its electron density into the aromatic ring making these ligands π-excessive as compared to benzene.

4.5. Comparison of binding to other cations

Gapeev et al. determined the binding energies of a number of main-group and transition metal cations to pyrrole using radiative association kinetics and ligand exchange methods [32]. For the $M^+(C_4H_5N)$ complexes, the binding of the alkali metal cations, except to Li^+, is significantly weaker than for all of the transition metal cations, V^+, Cr^+, Mn^+, Fe^+, Co^+, Ni^+, Cu^+, Mo^+, and W^+. The enhanced binding of transition metal cations arises because of the d orbital involvement in the binding, i.e., electron back-donation from the 3d orbitals of the transition metal cation into the π* orbitals of the aromatic ligand [72], and thus leads to partial covalent character in the binding. While for Li^+, the binding strength of pyrrole is comparable to that of Cr^+ and Mn^+ because of the small size of the cation and the higher degree of covalency in the binding of the $Li^+(C_4H_5N)$ complex. Similar to alkali metal cations, the binding of main group metal cations, Mg^+ and Al^+, is electrostatic in nature, and thus is weaker than binding to most transition metal cations and comparable to that of Cr^+ and Mn^+. Mg^+ and Al^+ bind to pyrrole more strongly than Na^+, K^+, Rb^+, Cs^+, and comparable to Li^+ because sp polarization in the Mg^+ and Al^+ complexes polarizes electron density 180° away from the metal cation–pyrrole binding interaction, and therefore allows the ligand to approach the metal cation with minimum electronic repulsion. For the $M^+(C_4H_5N)_2$ com-

plexes, alkali metal cation binding is weaker than the analogous mono-complexes for all of the transition metal cations. In contrast to the $M^+(C_4H_5N)$ complexes, the binding of the second pyrrole ligand to Mg^+ and Al^+ is weaker than Na^+. The change in the relative BDEs for the mono- and bis-complexes occurs as a result of the sp polarization of Mg^+ and Al^+ that enhances the binding in the mono-complexes diminishes as the second pyrrole ligand approaches, and thus weakens binding of the second pyrrole ligand.

The binding of organic cations is also electrostatic in nature, weaker than to transition metal cations and of comparable strength as the larger alkali metal cations, Rb^+ and Cs^+. Although NH_4^+ and K^+ have similar ionic radii, the binding of NH_4^+ to pyrrole is 75.4 kJ/mol stronger than to K^+ [73]. The enhanced binding likely arises as a result of the larger polarizability of NH_4^+, 8.75 Å^3, as compared to that of K^+, 5.35 Å^3. Thus a greater portion of the electron density of NH_4^+ can be polarized away from pyrrole and allow the pyrrole ligand to approach the positive charge center of NH_4^+ more closely. While for $N(CH_3)_4^+$, the repulsion between the bulky side chains and N is sufficiently strong that the positive charge center of $N(CH_3)_4^+$ gets shifted away from the center of the pyrrole ligand with one of the methyl groups pointing to the center of the electron density [73,74]. Thus, although the polarizability of $N(CH_3)_4^+$ is larger than that of NH_4^+, the binding of $N(CH_3)_4^+$ to pyrrole is 36.8 kJ/mol weaker than to NH_4^+, and weaker than to all of the other metal cations examined previously, indicating that the polarizability of the cation may not always be a the dominant factor that controls the strength of organic cation-π interactions.

The binding geometries of the M^+(pyrrole) complexes computed by Gapeev et al. are similar to those found here. The metal cation binds to the π cloud of the pyrrole ligand and is displaced from the center of the ring in the direction away from the nitrogen atom. The metal cation–pyrrole ring distances (M^+–$R_\perp$) were found to lie in the range from 1.912 and 2.416 Å, similar to the corresponding distance in the Li^+ and Na^+ complexes. However, the offset of the cation from the center of the ring varied more significantly than found for the alkali metal cations, from close to the center of the pyrrole ring to outside the perimeter of the ring as a result of the variation in size of the alkaline earth and transition metal cations and the involvement of the d electrons in the binding. Gapeev et al. also found a local minimum for the Cu^+(pyrrole) complex in which Cu^+ resides directly above the ring nitrogen atom however, this structure was computed to be 67 kJ/mol higher in energy that the ground state cation π complex.

5. Conclusions

The kinetic energy dependences of the CID of $M^+(C_4H_5N)_x$ complexes, where $M^+ = Na^+$, K^+, Rb^+, and Cs^+ for $x = 1$ and 2, and Li^+ for $x = 2$, with Xe are examined in a guided ion beam tandem mass spectrometer. The dominant pathway observed for all complexes is loss of an intact pyrrole ligand. The thresholds for these primary dissociation reactions are interpreted to yield 0 and 298 K BDEs. The molecular parameters needed for the analysis of experimental data as well as structures and theoretical estimates of the BDEs for the $M^+(C_4H_5N)_x$ complexes are obtained from theoretical calculations performed at the MP2(full)/6-311+G(2d,2p)//MP2(full)/6-31G* level of theory. The agreement between theory and experiment is very good for all complexes. The absolute M^+–(C_4H_5N) and $(C_4H_5N)M^+$–(C_4H_5N) BDEs are observed to decrease monotonically as the size of the alkali metal cation increases from Li^+ to Cs^+. Similarly, the differences in the BDEs for the mono- and bis-complexes are also observed to decrease with the size of the alkali metal cation. These trends are explained in terms of the electrostatic nature of the binding and changes in magnitude of the ligand–ligand interactions in the $M^+(C_4H_5N)_2$ complexes, respectively.

The influence of the N heteroatom on the cation-π binding is examined. The ability of the N heteroatom to delocalize electron density into the aromatic ring makes pyrrole and indole π-excessive as compared to benzene and is crucial to the enhancement of cation-π binding. Thus, pyrrole and indole are stronger π ligands than benzene and both the ion–quadrupole and ion-induced dipole interactions play a direct role in the binding of these complexes. Furthermore, trends in the binding of metal and organic cations to pyrrole suggest that the nature of the cation profoundly affects the optimized geometry and strength of binding. For alkali metal cations except Li^+ and organic cations, the cation-π interaction is purely electrostatic such that only the size, shape, and polarizability of the cation affect the binding geometry and strength. In contrast, binding of Li^+, Mg^+, Al^+, and the transition metal cations to pyrrole clearly establishes that the valence or core electron configurations are important to the binding, such that correlation, polarization, and hybridization of this electron density is crucial in the binding to the π ligand. As a result, binding to these metal cations is significantly enhanced, while trends in the strength of binding among these cations are determined by a balance of several factors.

Acknowledgements

This work is supported by the National Science Foundation, Grant CHE-0518262, and the American Chemical Society Petroleum Research Fund, Grant 40334-AC6.

References

[1] D.A. Dougherty, Science 271 (1996) 163.
[2] J.C. Ma, D.A. Dougherty, Chem. Rev. 97 (1997) 1303.
[3] S. Mecozzi, A.P. West Jr., D.A. Dougherty, J. Am. Chem. Soc. 118 (1996) 2307.
[4] S. Mecozzi, A.P. West Jr., D.A. Dougherty, Proc. Natl. Acad. Sci. U.S.A. 93 (1996) 10566.
[5] J.P. Gallivan, D.A. Dougherty, Proc. Natl. Acad. Sci. U.S.A. 96 (1999) 9459.
[6] H. Nicholson, W.J. Becktel, B.W. Matthew, Nature 336 (1988) 651.
[7] J. Sancho, L. Serrano, A.R. Fersht, Biochemistry 31 (1992) 2253.
[8] S.K. Burley, G.A. Petsko, Science 34 (1985) 15301.
[9] L. Serrano, M. Bycroft, A.R. Fesht, J. Mol. Biol. 218 (1991) 465.
[10] A.M. Devos, M. Ultsch, A.A. Kossiakoff, Science 255 (1992) 306.
[11] A. Karlin, Curr. Opin. Neurobiol. 3 (1993) 299.
[12] D.A. Stauffer, A. Karlin, Biochemistry 33 (1994) 6840.

[13] J.B. Mitchell, C.L. Nandi, I.K. McDonald, J.M. Thornton, S.L. Price, J. Mol. Biol. 239 (1994) 315.
[14] M.L. Raves, M. Harel, Y.P. Pang, I. Silman, A.P. Kozikowski, J.L. Sussman, Nat. Struct. Biol. 4 (1997) 57.
[15] W. Zhong, J.P. Gallivan, Y. Zhang, L. Li, H.A. Lester, D.A. Dougherty, Proc. Natl. Acad. Sci. U.S.A. 95 (1998) 12088.
[16] O. Donini, D.F. Weaver, J. Comput. Chem. 19 (1998) 1515.
[17] O.M. Cabarcos, C.J. Weinheimer, J.M. Lisy, J. Chem. Phys. 110 (1999) 8429.
[18] J. Sunner, K. Nishizawa, P. Kebarle, J. Phys. Chem. 85 (1981) 1814.
[19] B.C. Guo, J.W. Purnell, A.W. Castleman, Chem. Phys. Lett. 168 (1990) 155.
[20] R.L. Woodin, J.L. Beauchamp, J. Am. Chem. Soc. 100 (1978) 501.
[21] R.W. Taft, F. Anvia, J.-F. Gal, S. Walsh, M. Capon, M.C. Holmes, K. Hosn, G. Oloumi, R. Vasanwala, S. Yazdani, Pure Appl. Chem. 62 (1990) 17.
[22] P.B. Armentrout, M.T. Rodgers, J. Phys. Chem. A 104 (2000) 2238.
[23] V. Ryzhov, R.C. Dunbar, J. Am. Chem. Soc. 121 (1999) 2259.
[24] R. Amunugama, M.T. Rodgers, J. Phys. Chem. A 106 (2002) 9718.
[25] R. Amunugama, M.T. Rodgers, J. Phys. Chem. A 106 (2002) 5529.
[26] R. Amunugama, M.T. Rodgers, J. Phys. Chem. A 106 (2002) 9092.
[27] R. Amunugama, M.T. Rodgers, Int. J. Mass Spectrom. 227 (2003) 339.
[28] R. Amunugama, M.T. Rodgers, Int. J. Mass Spectrom. 222 (2003) 431.
[29] R. Amunugama, M.T. Rodgers, Int. J. Mass Spectrom. 227 (2003) 1.
[30] J.C. Amicangelo, P.B. Armentrout, J. Phys. Chem. A 104 (2000) 11420.
[31] H. Huang, M.T. Rodgers, J. Phys. Chem. A 106 (2002) 4277.
[32] A. Gapeev, C.-N. Yang, S.J. Klippenstein, R.C. Dunbar, J. Phys. Chem. A 104 (2000) 3246.
[33] N. Hallowita, D.R. Carl, P.B. Armentrout, M.T. Rodgers, manuscript in preparation.
[34] C. Ruan, Z. Yang, N. Hallowita, M.T. Rodgers, J. Phys. Chem. A 109 (2005) 11539.
[35] M. Meotner, C.A. Deakyne, J. Am. Chem. Soc. 107 (1985) 469.
[36] C.A. Deakyne, M. Meotner, J. Am. Chem. Soc. 107 (1985) 474.
[37] L. Bonomo, E. Solari, R. Scopelliti, C. Floriani, Chem. Eur. J. 7 (2001) 1322.
[38] E.S. Meadows, S.L. De Wall, L.J. Barbour, G.W. Gokel, J. Am. Chem. Soc. 123 (2001) 3092.
[39] J. Hu, L.J. Barbour, G.W. Gokel, Proc. Natl. Acad. Sci. U.S.A. 99 (2002) 5121.
[40] M.T. Rodgers, P.B. Armentrout, Int. J. Mass Spectrom. 185/186/187 (1999) 359.
[41] R. Amunugama, M.T. Rodgers, Int. J. Mass Spectrom. 195/196 (2000) 439.
[42] E.G. Brown, Ring Nitrogen and Key Biomolecules, Kluwer Academic Publishers, The Netherlands, 1998, p. 1.
[43] M.T. Rodgers, K.M. Ervin, P.B. Armentrout, J. Chem. Phys. 106 (1997) 4499.
[44] M.T. Rodgers, J. Phys. Chem. A 105 (2001) 2374.
[45] E. Teloy, D. Gerlich, Chem. Phys. 4 (1974) 417.
[46] D. Gerlich, Diplomarbeit, University of Freiburg, Federal Republic of Germany, 1971.
[47] D. Gerlich, in: C.-Y. Ng, M. Baer (Eds.), State-Selected and State-to-State Ion-Molecule Reaction Dynamics. Part I. Experiment Advances in Chemical Physics Series, vol. 82, Wiley, New York, 1992, p. 1.
[48] N.F. Dalleska, K. Honma, P.B. Armentrout, J. Am. Chem. Soc. 115 (1993) 12125.
[49] N. Aristov, P.B. Armentrout, J. Phys. Chem. 90 (1986) 5135.
[50] D.A. Hales, P.B. Armentrout, J. Cluster Sci. 1 (1990) 127.
[51] K.M. Ervin, P.B. Armentrout, J. Chem. Phys. 83 (1985) 166.
[52] N.F. Dalleska, K. Honma, L.S. Sunderlin, P.B. Armentrout, J. Am. Chem. Soc. 116 (1994) 3519.
[53] M.J. Frisch, G.W. Trucks, H.B. Schlegel, G.E. Scuseria, M.A. Robb, J.R. Cheeseman, J.A. Montgomery, T. Vreven, K.N. Kudin, J.C. Burant, J.M. Millam, S.S. Iyengar, J. Tomasi, V. Barone, B. Menucci, M. Cossi, G. Scalmani, N. Rega, G.A. Petersson, H. Nakatsuji, M. Hada, M. Ehara, K. Toyota, R. Fukuda, J. Hasegawa, M. Ishida, T. Nakajima, Y. Honda, O. Kitao, H. Nakai, M. Klene, X. Li, J.E. Knox, H.P. Hratchian, J.B. Cross, C. Adamo, J. Jaramillo, R. Gomperts, R.E. Stratman, P.Y. Yazyev, A.J. Austin, R. Cammi, C. Pomelli, J. Ochterski, P.Y. Ayala, K. Morokuma, G.A. Voth, P. Salvador, J.J. Dannenberg, V.G. Zakrzewski, S. Dapprich, A.D. Daniels, M.C. Strain, O. Farkas, D.K. Malick, D. Rabuck, K. Raghavachari, J.B. Foresman, J.V. Ortiz, Q. Cui, A.G. Baboul, S. Clifford, J. Cioslowski, B.B. Stefanov, G. Liu, A. Liashenko, P. Piskorz, I. Komaromi, R.L. Martin, D.J. Fox, T. Keith, M.A. Al-Laham, C.Y. Peng, A. Nanayakkara, M. Challacombe, P.M.W. Gill, B.G. Johnson, W. Chen, M.W. Wong, C. Gonzales, J.A. Pople, Gaussian 03, Revision D. 03, Gaussian, Inc., Pittsburgh, PA, 2003.
[54] P.J. Hay, W.R. Wadt, J. Chem. Phys. 82 (1985) 299.
[55] S.F. Boys, R. Bernardi, Mol. Phys. 19 (1979) 553.
[56] F.B. van Duijneveldt, J.G.C.M. van Duijneveldt-van de Rijdt, J.H. van Lenthe, Chem. Rev. 94 (1994) 1873.
[57] C. Adamo, V. Barone, J. Chem. Phys. 110 (1999) 6158.
[58] C. Adamo, M. Cossi, G. Scalmani, V. Barone, Chem. Phys. Lett. 307 (1999) 265.
[59] C. Van Caillie, R.D. Amos, Chem. Phys. Lett. 328 (2000) 446.
[60] S.M. Smith, A.N. Markevitch, D.A. Romanov, X. Li, R.J. Levis, H.B. Schlegel, J. Phys. Chem. A 108 (2000) 11063.
[61] E.D. Glendening, J.K. Badenhoop, A.E. Reed, J.E. Carpenter, F. Weinhold, NBO Version 3.1, Theoretical Chemistry Institute, University of Wisconsin, Madison, 1995.
[62] F. Muntean, P.B. Armentrout, J. Chem. Phys. 115 (2001) 1213.
[63] T.S. Beyer, D.F. Swinehart, Comm. Assoc. Comput. Mach. 16 (1973) 379.
[64] S.E. Stein, B.S. Rabinovitch, J. Chem. Phys. 58 (1973) 2438.
[65] S.E. Stein, B.S. Rabinovitch, Chem. Phys. Lett. 49 (1977) 183.
[66] F.A. Khan, D.E. Clemmer, R.H. Schultz, P.B. Armentrout, J. Phys. Chem. 97 (1993) 7978.
[67] W.J. Chesnavich, M.T. Bowers, J. Phys. Chem. 83 (1979) 900.
[68] See for example, Fig. 1 in N.F. Dalleska, K. Honma, P.B. Armentrout, J. Am. Chem. Soc. 115 (1993) 12125.
[69] P.B. Armentrout, J. Simons, J. Am. Chem. Soc. 114 (1992) 8627.
[70] M.T. Rodgers, P.B. Armentrout, Int. J. Mass Spectrom. submitted for publication.
[71] S.D.M. Chinthaka, Y. Chu, N.S. Rannulu, M.T. Rodgers, J. Phys. Chem. A 110 (2006) 1426.
[72] C.W. Bauschlicher Jr., H. Partridge, S.R. Langhoff, J. Phys. Chem. 96 (1992) 3273.
[73] D. Kim, S. Hu, P. Tarakeshwar, S.S. Kim, J.M. Lisy, J. Phys. Chem. A 107 (2003) 1228.
[74] T. Liu, J. Gu, X.J. Tan, W.L. Zhu, X.M. Luo, H.L. Jiang, R.Y. Ji, K.X. Chen, I. Silman, J.L. Sussman, J. Phys. Chem. A 105 (2001) 5431.